Journal of Power Sources 208 (2012) 170–175

Contents lists available at SciVerse ScienceDirect

Journal of Power Sources

journal homepage: www.elsevier.com/locate/jpowsour

Short communication

Carbon supported cobalt oxide nanoparticles–iron phthalocyanine as alternative cathode catalyst for oxygen reduction in microbial fuel cells

Jalal Ahmed [a], Yong Yuan [b,c,*], Lihua Zhou [d], Sunghyun Kim [a,**]

[a] Department of Bioscience and Biotechnology, Konkuk University, Seoul 143-701, Republic of Korea
[b] Guangdong Institute of Eco-environmental and Soil Sciences, Guangzhou 510650, China
[c] State Key Laboratory of Soil Erosion and Dryland Farming on the Loess Plateau, Institute of Water and Soil Conservation, Chinese Academy of Sciences & Ministry of Water Resources, Yangling 712100, China
[d] Faculty of Chemical Engineering and Light Industry, Guangdong University of Technology, Guangzhou 510006, China

ARTICLE INFO

Article history:
Received 17 January 2012
Accepted 1 February 2012
Available online 10 February 2012

Keywords:
Cobalt oxide nanoparticles
Iron phthalocyanine
Platinum
Microbial fuel cell

ABSTRACT

The high cost and limited resources of precious metals as oxygen reduction catalysts (ORR) hindered the widespread use of microbial fuel cells (MFCs) in practice. Here, the feasibility of metal oxide assisted metal macrocyclic complex was investigated as a catalyst for ORR in an air-cathode MFC. Electrochemical results revealed that cobalt oxide (CoOx) incorporation increased the ORR activity of iron phthalocyanine (FePc). In MFCs, the maximum power density of 654 ± 32 mW m^{-2} was achieved from the C–CoOx–FePc cathode, which was 37% higher than the power density of carbon supported FePc (C–FePc). The voltage output of the MFC only decreased to 85% of its initial voltage after 50 cycles, suggesting that the synthesized catalyst showed acceptable long-term stability. The voltage drop partially resulted from the covering of biofilm on the catalyst layer. This work provided a potential alternative to Pt in MFCs for sustainable energy generation.

1. Introduction

Microbial fuel cells (MFCs) are an emerging green technology that employs the catalytic activity of microorganisms to degrade a wide range of organic matter and simultaneously generate electricity [1,2]. MFCs have the potential to revolutionize water treatment regarding its ability for degrading organic compounds in various wastes [3]. Although being a promising biotechnology, the application of MFCs in the real field is limited by its small-scale power output and high cost. Therefore, a considerable effort has been implied on improving the performances of MFCs by optimizing different operational parameters, for example, electrode materials [4], electrode surface area and spacing [5,6], temperature [7,8], substrate flow [9,10] and others.

Significant progress has been made in the development of MFCs due to intensive research in this field. Further improvement in MFC design, materials, and uninterrupted long time operation are still needed. Specifically, efforts are required in order to replace Pt as the oxygen reduction reaction (ORR) catalyst in the cathode. Oxygen is considered one of the most suitable electron acceptor in MFCs for its inherent high oxidation potential, sustainability and passive aeration on the cathode that does not require an external energy input [11]. However, the sluggish kinetics of ORR at neutral pH accounts for a high overpotential. Although platinum (Pt) can be used as an efficient catalyst towards the electroreduction of oxygen, Pt remains impractical due to its over high cost, scarcity and prone to be poisoned while the wastewater treatment [12]. Thus, Pt should be replaced in the MFC for a sustainable, cost-effective and widespread application of MFC.

Iron phthalocyanine (FePc) known as a good oxygen reduction catalyst had been widely examined as an alternative to Pt in MFCs [12–16]. Prior to being employed to the cathode, FePc was usually supported on carbon materials with a high surface area and high electrical conductivity. Previous studies showed that the catalytic activity of FePc was greatly affected by the support materials. For instance, Yuan et al. [17,18] revealed that polyaniline or amino functionalized carbon nanotube supported FePc had an improved catalytic activity toward ORR in the MFCs. The enhanced catalytic activity likely resulted from the synergetic effects of both FePc and the supporting materials. Cobalt oxide has specifically been found to catalyze the disproportionation reaction of hydrogen peroxide, an important undesirable intermediate in oxygen electroreduction, by which intensive attention has been attracted to form new ORR catalysts by integrating CoOx with other catalysts, such as Au, MnO_2 [19,20]. Very recently, Goubert-Renaudin et al. [21] reported that

* Corresponding author at: Guangdong Institute of Eco-environmental and Soil Sciences, Guangzhou 510650, China. Tel.: +86 20 87025101; fax: +86 20 87025101.
** Corresponding author. Tel.: +82 2 4503378; fax: +82 2 4562744.
E-mail addresses: yuanyong@soil.gd.cn (Y. Yuan), skim100@konkuk.ac.kr (S. Kim).

0378-7753/$ – see front matter © 2012 Elsevier B.V. All rights reserved.
doi:10.1016/j.jpowsour.2012.02.005

the catalytic activity of cobalt porphyrin could be also increased by being integrated with cobalt oxides. It was the possible reason that the surface of transition metal oxides favored electron localization over the bulk itinerant electron state, which increased the activity of the catalyst for ORR [22]. However, the feasibility of this type of catalyst has not been previously examined in fuel cells. In this present study, a carbon cobalt oxide (C–CoOx) precursor was synthesized by heating a metal compound and carbon black, followed by the FePc adsorption to produce a C–CoOx–FePc catalyst. The catalyst was characterized by X-ray spectroscopy and electrochemical techniques, and its application was justified in the air cathode MFC using passive air as oxygen supply.

2. Materials and methods

2.1. Synthesis of carbon supported metal oxide–metal phthalocyanine composite

Cobalt nitrate hexahydrate ($Co(NO_3)_2{\cdot}6H_2O$) crystal was finely crushed in a mortar. Carbon particles (Vulcan XC-72, Cabot, USA) and fine $Co(NO_3)_2{\cdot}6H_2O$ powder were mixed in the mortar at a ratio that 20 wt.% Co was loaded in the carbon particles. These composite mixture was heated for 1 h at 130 °C that was above the melting and decomposition temperature of $Co(NO_3)_2$ to ensure the impregnation of cobalt salt into the carbon particles and decomposed to CoOx, then heated for another 2 h after raising the temperature up to 400 °C. Heating at this higher temperature allowed graphitic structural rearrangement of carbon which was somewhat disordered [23]. The resulted C–CoOx was cool down to room temperature. FePc (20 mg) was suspended in 20 mL chloroform by sonication. C–CoOx (200 mg) was dispersed to FePc suspension and stirred for 4 h under argon gas. The mixture was filtered under vacuum, rinsed and dried at 30 °C. This metal oxide assisted macrocyclic complex was characterized using different techniques.

2.2. Physical characterization

X-ray photoelectron spectroscopy (XPS) analyses were performed in an AXIS Nova (Kratos Inc., UK) with hemispherical energy analyzer using monochromatic light. Powder samples were dispersed on copper tape. Transmission electron microscopy (TEM) images were taken in a FE TEM (JEM2100F TEM, JEOL Ltd., Japan). Samples were sonicated in ethanol before being spread on the copper grid (Lacey F/C grid, 300 mesh, 01883-F, Ted Pella Inc., Sweden) and dried under vacuum.

2.3. Electrochemical measurement

Linear sweep voltammetry (LSV) was measured on a glassy carbon (GC) electrode using Autolab (PGSTAT 30, ECO CHEM, Netherlands) potentiostat with a conventional three-electrode system to investigate the ORR activity of the catalyst. The catalyst coated GC electrode (3 mm diameter) was used as the working electrode, Pt wire as the counter and saturated calomel electrode (SCE) as the reference electrode, respectively. To prepare the working electrode, the catalyst ink (2 μl) prepared by dispersing 2 mg samples in 0.4 mL ethanol and 0.1 mL of 5% nafion solution, was dropped on the GC electrode. The electrode was dried at 30 °C for 2 h. Data was taken in 50 mM phosphate buffer (pH 7.0) electrolyte at 5 mV s^{-1} scan rate.

2.4. MFC construction and inoculation

MFCs were constructed as described by Cheng and coauthors [24] with little modification. A cylindrical shape (3.0 cm Ø × 2.0 cm L) reactor was made from acryl with a final volume of 14 mL. The space of anode and cathode was 2.0 cm. A non wet proof carbon cloth (type A) for anode and 30% wet proof carbon cloth (type B) used for cathode were collected from Fuel Cell Earth LLC Inc. (USA). The cathode catalyst layer was prepared as descried previously [25]. Briefly, the catalyst slurry was prepared by mixing 1 mg synthesized catalyst with 1 μl water, and then nafion solution (5%, 7 μl) and Isopropyl alcohol (IPA) (2 μl) was added to the slurry to prepare a homogenous catalyst ink mixture. This composite mixture was applied on the one side of air cathode and dried overnight at room temperature. The MFCs were inoculated by mixing 2 mL anaerobic sludge collected from the Liede sewage plant (Guangzhou, China) with 12 mL culture media. Culture media was 1 g L^{-1} sodium acetate solution in 50 mM phosphate buffer containing 12.5 mL L^{-1} mineral solution and 5 mL L^{-1} vitamin solution. MFCs were operated in batch mode with 1 kΩ external resistance and were subjected to at least five charging–discharging periods before collecting data. The polarization curve was then constructed by discharging the cell with external loads of various resistance values from 5000 to 50 Ω. The cell voltage outputs were continuously monitored using a 16-channel voltage collection instrument (AD8223, China). Each electrode potential was recorded with respect to a saturated calomel electrode (SCE) using a multimeter. All data were recorded from three different reactors and the average result was taken as a final with standard deviation.

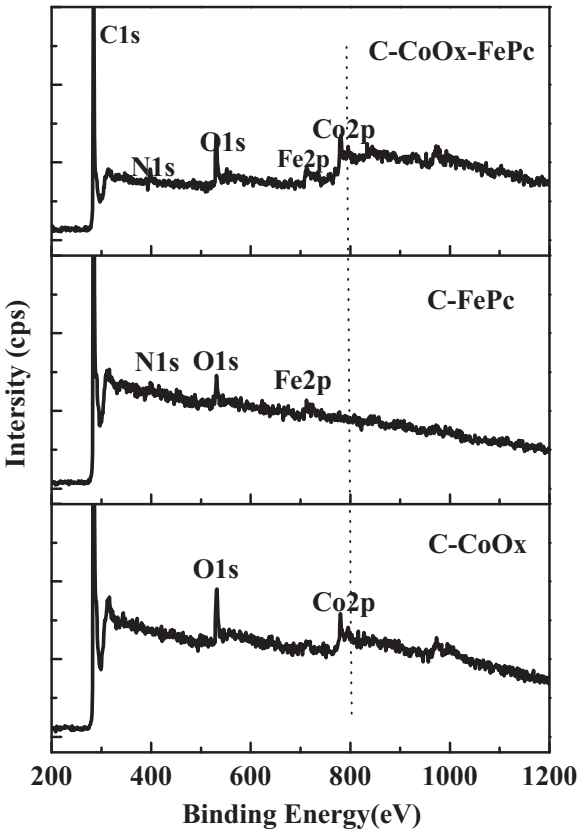

Fig. 1. XPS analysis results for different composite catalysts.

3. Results and discussion

3.1. Characterization of C–CoOx–FePc

The synthesized C–CoOx–FePc composite was characterized by using XPS and TEM. The XPS spectra of C–CoOx–FePc and controls were shown in Fig. 1. Co 2p peaks at 779 eV due to the characteristic binding energy of cobalt clearly appeared in panel A and C, but

panel B has no such peak in this region as no cobalt was present. FePc loaded samples in panel A and B had N 1s peak at 399.5 eV for metal–N bonding in the metal centered phthalocyanine. This peak completely absent in panel C containing only cobalt oxide loaded carbon particles. It was worth mentioning that no peaks were observed for Co 2p3/2 at 852 eV which was the characteristic binding energy for zero valent metallic cobalt [26], and O 1s peak at 529.4 eV which was the characteristic peak of CoO [27]. This result indicated that the heat treatment led to the metal oxide incorporation and not to the metallic transformation.

Formation of metal oxide nanoparticle was confirmed from the representative TEM images. As shown in Fig. 2A, the darkest spot that appeared inside the carbon particles represented a clear indication of metallic incorporation inside the carbon structure. Fig. 2B showed the homogeneous dispersion of FePc on the carbon particles. Fig. 2C was a representative image of C–CoOx–FePc, which appeared with a deep dark spot at the center surrounded with light shade, suggesting that the CoOx nanoparticles were encapsulated with the macrocyclic complex.

3.2. Electrochemical characterization of C–CoOx–FePc catalyst

The ORR activity of C–CoOx–FePc was analyzed by CV and LSV, which was compared with C–CoOx, C–FePc, and C–Pt catalysts to determine the function of CoOx loading on the carbon supported catalyst. As shown in Fig. 3A and B, a new reduction peak was observed when the CV was conducted in O_2-saturated solution with various electrodes. A reduction peak at −0.015 V (vs. SCE) appeared at the C–CoOx–FePc electrode, which was more positive than those at the C–CoOx electrode (−0.31 V vs. SCE) and the C–FePc electrode (−0.12 V vs. SCE) (Fig. 3B and D). The positive shifting of the electroreduction peak as well as the increased peak current density demonstrated that the integration of CoOx with FePc attributed for the improved ORR catalytic activity. The chronoamperometric measurements of the ORR over C–CoOx–FePc, C–CoOx, C–FePc, and C–Pt catalysts at 0 V (vs. SCE) showed that the steady-state current density for the C–CoOx–FePc was significant higher compared to C–CoOx and C–FePc (Fig. 3E and F). This was in agreement with the CVs and LSV results. It was revealed that cobalt oxide was an efficient synergistic component for other ORR catalysts due to the capability of catalyzing the disproportionation reaction of the intermediater in oxygen electroreduction. A dual-site mechanism had been proposed for cobalt based ORR catalysts (i.e. cobalt–polypyrrole/C), in which oxygen was reduced to peroxide at Co–N complex and further reduced to OH^- at CoOx/Co site under an alkaline condition [28]. Herein, oxygen was firstly reduced to peroxide at FePc complex, and then reduced to H_2O at CoOx/Co site. In this way, the synergistic coupling between CoOx and FePc was essential for the high ORR activity of the hybrid. Meanwhile, Lin et al. [19] demonstrated that CoOx had high affinity towards oxygen, which might favor the chemisorptions of oxygen molecules on the catalyst surface. As a result, the ORR catalytic activity of CoOx-based catalysts was greatly enhanced.

3.3. Performances of the MFCs with various cathodes

Power densities and polarization curves were studied by using polarization curve for different catalysts loaded air cathodes as shown in Fig. 4A. The MFC with the C–CoOx–FePc cathode produced a power density of 654 ± 32 mW m^{-2}. However, power densities with other catalysts were 554 ± 27, 412 ± 20, and 271 ± 13 mW m^{-2} for C–CoOx, C–FePc and carbon powder, respectively, which were all lower than the power density produced for the MFC with C–CoOx–FePc, suggesting that the integration of CoOx with FePc was feasible to improve the catalytic ORR activity of FePc based cathode in fuel cells. All the results were compared with the same amount of catalyst loading on the air cathode and all other conditions were the same. The developed power density from the C–CoOx–FePc cathode was comparable with those derived from polymer or carbon nanotube integrated FePc cathodes [17,18]. Fig. 4B. showed the curves of individual electrode potentials versus current densities. It was observed that the potential variations for

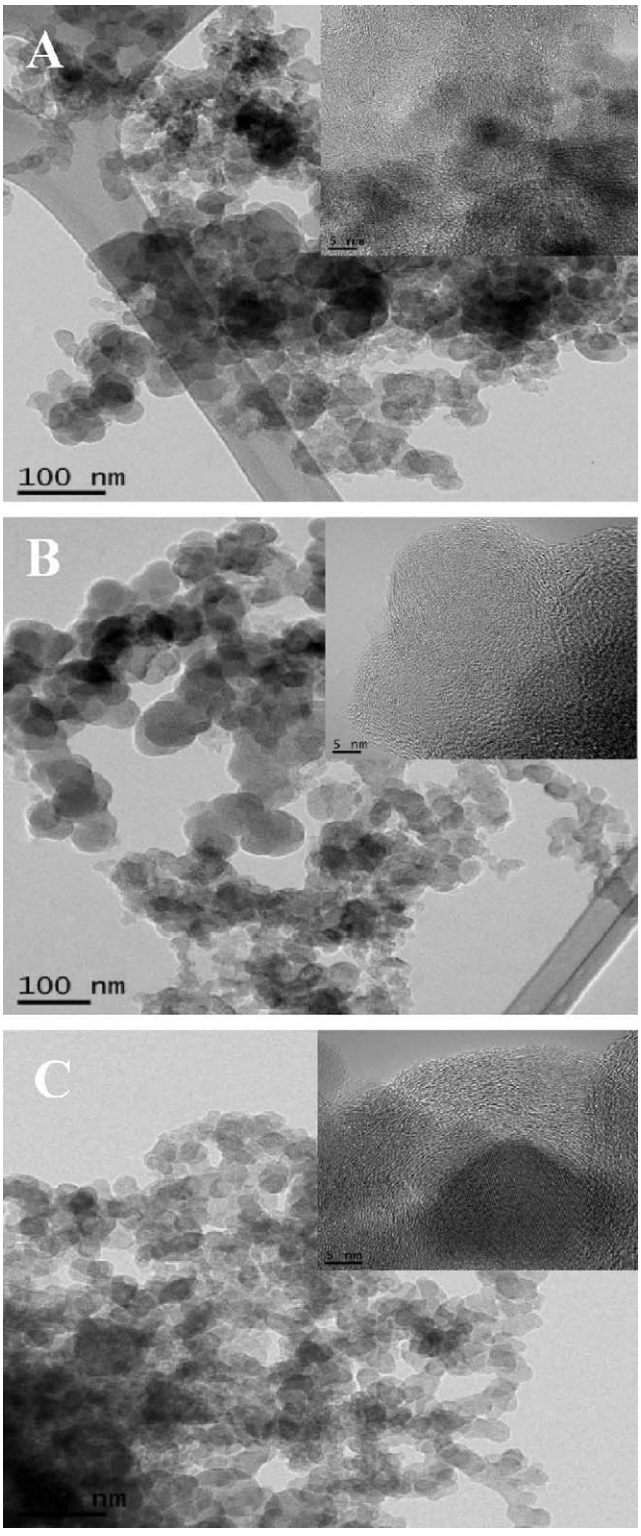

Fig. 2. TEM image of typical non-precious metal oxide catalyst nanostructure (A) C–CoOx, (B) C–FePc and (C) C–CoOx–FePc involving metal oxide aggregate inside graphitic nanoshells.

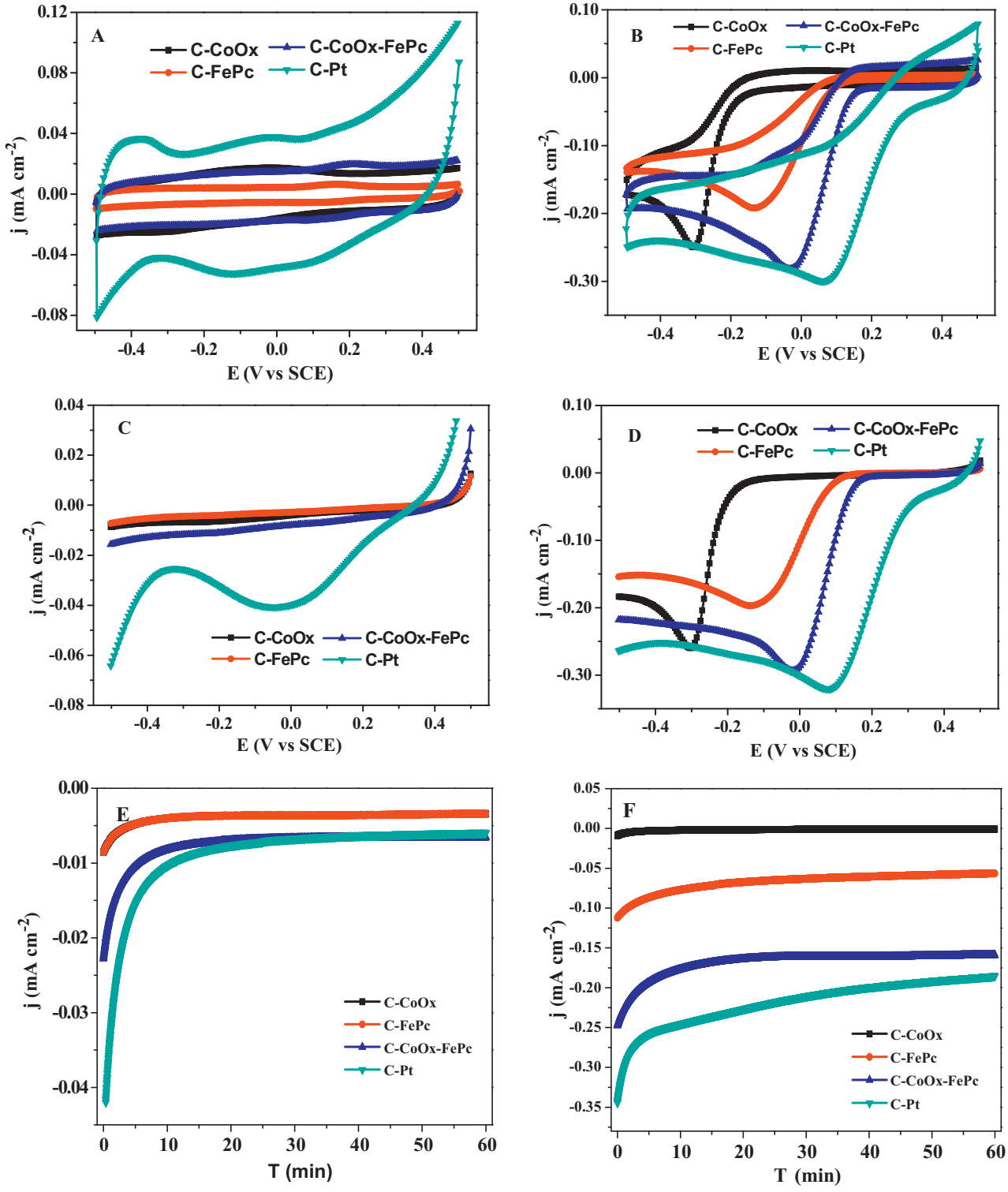

Fig. 3. Cyclic voltammograms in nitrogen-saturated (A) and oxygen-saturated (B) PBS buffer at 5 mV s^{-1}; linear sweep voltammograms in nitrogen-saturated (C) and oxygen-saturated (D) PBS buffer; chronoamperograms at 0 V (vs SCE) in nitrogen-saturated (E) and oxygen-saturated (F) PBS buffer.

cathode was much more distinctive as compared with the anode potential variation for various MFCs. Anode potentials were almost same for different MFCs whereas cathode potentials varied in a wide difference. The variation in cathode potentials was mainly due to the efficiency of the different catalysts towards oxygen reduction. Besides, the catalyst loading had an apparent effect on the power output. As shown in Fig. 5, the highest power density was obtained with 4 mg cm^{-2} C–CoOx–FePc loading at the cathode. Contrary to our expectation, the higher amount of catalyst resulted in the lower power density. This might be due to a decrease in oxygen diffusion rate on highly packed surface, which then led to an increase in the diffusion resistance of the cathode.

Other parameters of the MFCs with various cathodes were also studied in terms of open circuit voltage (OCV), coulombic efficiency (CE), and internal resistance. As depicted in Table 1, the MFCs with different cathodic oxygen reduction catalysts displayed different

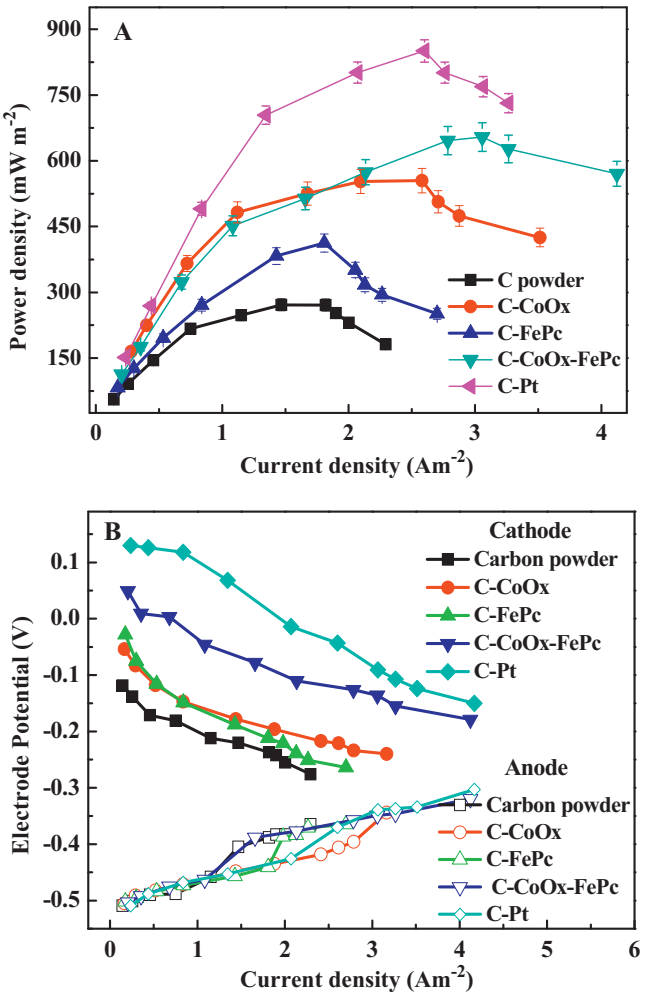

Fig. 4. Power densities versus current densities curves with various cathodes (A) and electrode potentials (vs. SCE) as a function of different cathodes (B).

performances. The MFC with C–CoOx–FePc cathodes had a smaller internal resistance and higher OCP as well as CE in comparison with C–CoOx and C–FePc cathode, which could attribute to the higher electrocatalytic oxygen reduction activity of the C–CoOx–FePc. However, the internal resistance with the C–CoOx–FePc cathode

Table 1
Comparison of different parameters of various cathode materials (data are presented as mean ± SD, (n = 3)).

Cathode	R_{In} (Ω)	OCV (mV)	P_{max} (mW m^{-2})	CE (%)
C–Pt	328	820 ± 41	850 ± 42	28
C powder	449	520 ± 26	271 ± 13	25
C–CoOx	443	750 ± 37	555 ± 27	26
C–FePc	440	650 ± 32	412 ± 20	23
C–CoOx–FePc	338	695 ± 34	654 ± 32	27

(338 Ω) is higher and OCV (695 mV) is lower than those (328 Ω and 820 mV) with the Pt cathode, suggesting that the catalytic activity of the C–CoOx–FePc was still lower than that of the Pt. As mentioned above, the high cost of MFCs is limiting its practical applications. Thus, it is very urgent to replace the Pt in the cathode by using other efficient ORR catalyst with low prices. Although the energy output of the C–CoOx–FePc cathode was lower than that of the Pt cathode, the power per cost of the C–CoOx–FePc cathode (11 mW $^{-1}$) was 3.7 times higher than that of the Pt cathode (3 mW $^{-1}$). With respect to this big economic advantage and viability, C–CoOx–FePc was believed to be a potential alternative to Pt in MFCs for practical applications.

3.4. Stability of the catalyst

Long term stability test was conducted to confirm the longevity of the catalyst. More than 50 full discharging–charging cycles were tested at the MFC with 1 kΩ external loading during over 2 months. It was found that voltage generation gradually decreased to 85% of its initial voltage after 60 days (see Fig. 6). Following the same trend as described by Zhang et al. [29], the voltage decreased as the development of cathodic biofilm. They had claimed that accumulation of biomass on the cathode hindered the proton diffusion and also introduced activation resistance per surface area, consequently decreased the voltage output. The similar voltage development trend was observed in the MFC with the C–CoOx–FePc cathode after 40 cycle's operations. Thereafter, the cathodic biofilm was scrapped off from the cathode and the MFC was reassembled. As can be seen in Fig. 6, in the new cycle the voltage output was restored, but it only reached to 88–90% of its initial voltage. This observation revealed that, like most of the cathode catalysts, it also poisoned or deactivated to some extent from its initial activity after a long term operation.

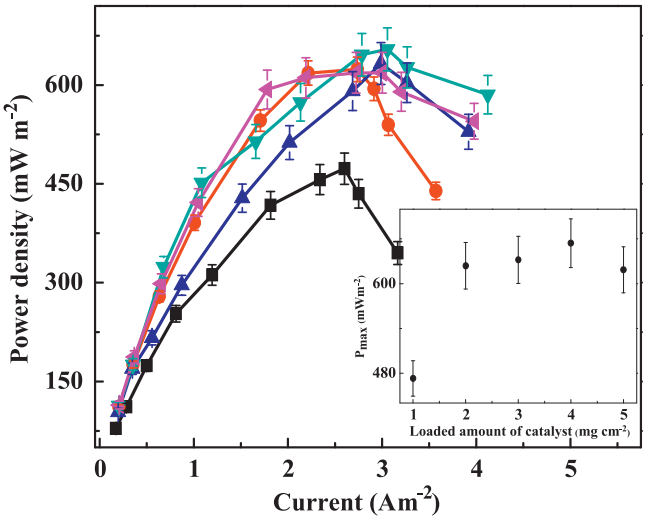

Fig. 5. Maximum power densities as a function of catalyst loading amount.

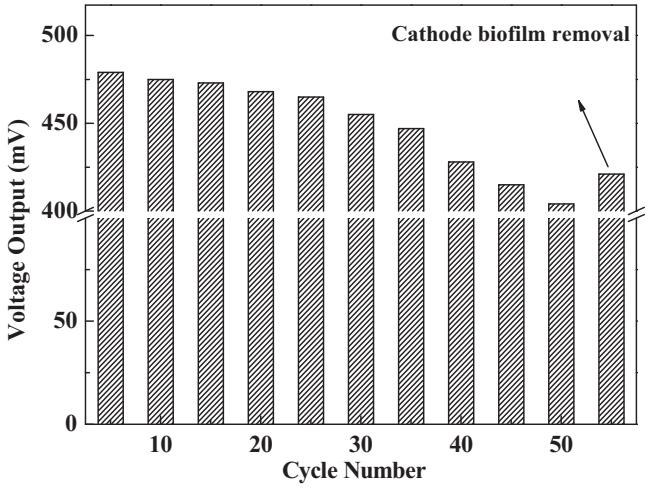

Fig. 6. Voltage generation in individual cycles under 1 kΩ external load for long term operations.

4. Conclusions

A rather inexpensive yet efficient cathode catalyst was synthesized and fabricated into the air-cathode single-chamber MFC. The catalyst contained multimetal center (cobalt and iron), which showed higher catalytic activity toward ORR than the catalyst with a single iron center. As a result, the MFC with the synthesized catalyst cathode produced a power density $654 \pm 32\,\mathrm{mW\,m^{-2}}$, which was 37% higher than the catalyst in the absence of cobalt oxide. In addition, the long-term stability and low cost was the additional feature to consider this catalyst a potential alternative candidate to Pt in the MFC.

Acknowledgements

This work was supported by the National Nature Science foundation of China (No. 41101211), the Nature Science foundation of Guangdong Province, China (No. S2011010004991), the Youth Foundation of Guangdong Academy of Sciences (No. qnjj201005), the National Research Foundation of Korea (NRF) grant funded by the Korea government (No. 2011-0017923), and the foundation of the State Key Laboratory of Soil Erosion and Dryland Farming on the Loess Plateau (Grant No. 10501-253).

References

[1] B.E. Logan, B. Hamelers, R. Rozendal, U. Schröder, J. Keller, S. Freguia, P. Aeltermann, W. Varstraete, K. Rabaey, Environ. Sci. Technol. 40 (2006) 5181–5192.
[2] U. Schröder, Phys. Chem. Chem. Phys. 9 (2007) 2619–2629.
[3] B.E. Logan, Wat. Sci. Technol. 52 (2005) 31–37.
[4] Y. Yuan, S.H. Kim, Bull. Korean Chem. Soc. 29 (2008) 168–172.
[5] S.E. Oh, B.E. Logan, Appl. Micbiol. Biotechnol. 70 (2006) 162–169.
[6] M.M. Ghangreker, V.B. Shinde, Biresour. Technol. 98 (2007) 2879–2885.
[7] H. Liu, S. Cheng, B.E. Logan, Environ. Sci. Technol. 39 (2005) 5488–5493.
[8] S.A. Patil, F. Harnisch, B. Kapadnis, U. Schröder, Biosen. Bioelectron. 26 (2010) 803–808.
[9] I. Ieropoulos, J. Winfield, J. Greenman, Biresour. Technol. 101 (2010) 3520–3525.
[10] J.Y. Nam, H.W. Kim, K.H. Lim, H.S. Shin, Biresour. Technol. 101 (2010) S33–S37.
[11] L. Fu, S.J. You, G.Q. Zhang, F.L. Yang, X.H. Fang, Z. Gong, Bioesens. Bioelctron. 26 (2011) 1975–1979.
[12] S. Cheng, H. Liu, B.E. Logan, Environ. Sci. Technol. 40 (2006) 364–369.
[13] F. Zhao, F. Harnisch, U. Schröder, F. Schölz, P. Bogdanoff, I. Herrmann, Electrochem. Commun. 7 (2005) 1405–1410.
[14] L. Birry, P. Mehta, F. Jaouen, J.-P. Dodelet, S.R. Guiot, B. Tartakovsky, Electrochim. Acta 56 (3) (2011) 1505–1511.
[15] J. Ma, J. Wang, Y. Liu, J. Power Sources 172 (2007) 220–224.
[16] E.H. Yu, S. Cheng, K. Scott, B.E. Logan, J. Power Sources 171 (2007) 275–281.
[17] Y. Yuan, J.S. Ahmed, Kim, J. Power Sources 196 (2011) 1103–1106.
[18] Y. Yuan, B. Zhao, Y. Jeon, S. Zhong, S. Zhou, S.H. Kim, Bioresour. Technol. 102 (2011) 5849–5854.
[19] H.F. Lin, W. Tang, A. Kleiman-Shwarstein, E.W. McFarland, J. Electrochem. Soc. 155 (2008) B200–B206.
[20] M. Mahmoud, T.A.G. Allah, K.M. El-Katib, F. El-Gohary, Bioresour. Technol., in press.
[21] N.S. Goubert-Renaudin, X. Zhu, A. Wieckowski, Electrochem. Commun. 12 (2010) 1457–1461.
[22] J. Suntivich, H.A. Gasteiger, N. Yabuchi, H. Nakanishi, J.B. Goodenough, Y.S. Horn, Nat. Chem. 3 (2011) 546–550.
[23] G. Wu, K.L. More, C.M. Johnston, P. Zelanay, Science 332 (2011) 443–447.
[24] H. Liu, B.E. Logan, Environ. Sci. Technol. 38 (2004) 4040–4046.
[25] S. Cheng, H. Liu, B.E. Logan, Electrochem. Commun. 8 (2006) 489–494.
[26] J.F. Moulder, W.F. Stickle, P.E. Sobol, K.D. Bomben, Handbook of X-ray Photoelectron Spectroscopy, Physical Electronics Inc., Chanhassen, MN, 1995.
[27] S.C. Petito, M.E. Marsh, G.A. Carson, M.A. Langel, J. Mol. Catal. A: Chem. 281 (2008) 49–58.
[28] T.S. Olson, S. Pylypenkov, P. Atanassov, J. Phys. Chem. C 114 (2010) 5049–5059.
[29] X. Zhang, S. Cheng, X. Wang, X. Huang, B.E. Logan, Environ. Sci. Technol. 43 (2009) 8456–8461.